Journal of Alloys and Compounds 505 (2010) 239–242

Contents lists available at ScienceDirect

Journal of Alloys and Compounds

journal homepage: www.elsevier.com/locate/jallcom

Co-precipitation synthesis and photoluminescence properties of $(Ca_{1-x-y},Ln_y)MoO_4$: xEu^{3+} (Ln = Y, Gd) red phosphors

Yang Yu-Ling[a], Li Xue-Ming[a,*], Feng Wen-Lin[a,b,c], Li Wu-Lin[a], Tao Chuan-Yi[a]

[a] College of Chemistry and Chemical Engineering, Chongqing University, Chongqing 400044, China
[b] Department of Applied Physics, Chongqing University of Technology, Chongqing 400054, China
[c] International Centre for Materials Physics, Chinese Academy of Sciences, Shenyang 110016, China

ARTICLE INFO

Article history:
Received 9 May 2010
Received in revised form 3 June 2010
Accepted 10 June 2010
Available online 18 June 2010

Keywords:
Co-precipitation
Red phosphor
Photoluminescence
$(Ca_{1-x-y},Ln_y)MoO_4$: xEu^{3+} (Ln = Y Gd)

ABSTRACT

$(Ca_{1-x-y},Ln_y)MoO_4$: xEu^{3+} (Ln = Y, Gd) red phosphors were prepared by co-precipitation method with NH_4HCO_3–$NH_3{\cdot}H_2O$ system as the precipitating agent. X-ray diffraction (XRD), Fourier transform infrared spectrometer (FT-IR), and energy-dispersive X-ray spectrometer (EDS) were used to characterize the structure and composition of the phosphors. The synthesized $(Ca_{1-x-y},Ln_y)MoO_4$: xEu^{3+} have scheelite structure with pure phase. FT-IR spectra show strong absorption peaks between 914 and 730 cm^{-1} which are assigned to the vibration of O–Mo–O in MoO_4^{2-} tetrahedron. The EDS analysis reveals that the red phosphors have been successfully prepared by co-precipitation method according to theoretic ratio. Photoluminescence spectra show a red emission around 614 with 394 and 464 nm excitation, which is match well with the output wavelength of commercial ultraviolet and blue LED chips. The luminescent intensity of $(Ca,Ln)MoO_4$: Eu^{3+} is obviously higher than that of $CaMoO_4$: Eu^{3+}.

1. Introduction

Due to the advantages of energy-saving, pollution-free, long lifetime and so on, the phosphor-converted white-light emitting diodes (W-LEDs) are widely considered as the next generation of solid-state illumination materials after the incandescent and fluorescent lamps [1]. Red phosphor plays an important role in the realization process of W-LEDs. It not only overcomes the shortcoming of poor color rendering index because of deficiency red in the white light which is generated by combining YAG: Ce yellow phosphor with blue LED, but also is an important component of tricolor (red, green and blue) phosphors. However, nowadays the widely used red phosphor, such as Y_2O_2S: Eu^{3+}, holds a low light-emitting efficiency, large light decay and unstable chemical property which seriously affect the lifetime and efficiency of W-LEDs [2]. Therefore, it is crucial to develop a novel red phosphor with high luminance, small full width at half maximum and low-light decline at the excitation of near ultraviolet light and blue light.

Recently, the Eu^{3+} doped molybdate compounds have attracted much attention for their excellent thermal and chemical stability [3–5]. Hu et al. [6] prepared $CaMoO_4$: Eu^{3+} red phosphor by solid-state method, the result of which shows red light emission of the phosphor is 5 times greater than that of traditional red phosphor Y_2O_2S: Eu^{3+}. However, its luminous efficiency still cannot meet the needs of W-LEDs [7]. The Y and Gd are particularly suitable for host material for the preparation of phosphor because of their optical inert [8]. Haque et al. [9] introduces the Y^{3+} into $NaCaY(MoO_4)_3$: Eu phosphor and finds that the emission intensity is higher than that of $CaMoO_4$: Eu. The study of $Li_3Ba_2Ln_{3-x}Eu_x(MoO_4)_8$ (Ln = La, Gd, Y) also indicates that the phosphor has strong red light at 616 nm [10]. In $(Ca_{1-x-y},Ln_y)MoO_4$: xEu^{3+} red phosphor, the partial sit of Ca^{2+} is replaced by Ln^{3+} which results in some changes in the lattice structure around the luminescent center ions Eu^{3+}, and obviously enhance the luminescent intensity comparable with the $CaMoO_4$: Eu^{3+}. In addition, the chemical co-precipitation method has the characteristic of the particle with good chemical uniformity and morphologies, which is favorable to luminescent property for less contamination or fewer dead layers on the phosphor surface [11].

In this paper, we discuss co-precipitation synthesis of $(Ca_{1-x-y},Ln_y)MoO_4$: xEu^{3+} (Ln = Y, Gd) phosphors. The structure, composition and photoluminescence property of the phosphors have been investigated and the best content of Y and Gd in $(Ca_{1-x-y},Ln_y)MoO_4$: xEu^{3+} has also been discussed, and the luminescence intensity of $(Ca_{1-x-y},Ln_y)MoO_4$: xEu^{3+} has been compared with that of $CaMoO_4$: Eu^{3+} phosphor. One can find that the luminescent intensity of $(Ca,Ln)MoO_4$: Eu^{3+} is obviously higher than that of $CaMoO_4$: Eu^{3+}.

* Corresponding author. Tel.: +86 23 65105659; fax: +86 23 65105659.
E-mail address: xuemingli@cqu.edu.cn (L. Xue-Ming).

0925-8388/$ – see front matter.
doi:10.1016/j.jallcom.2010.06.037

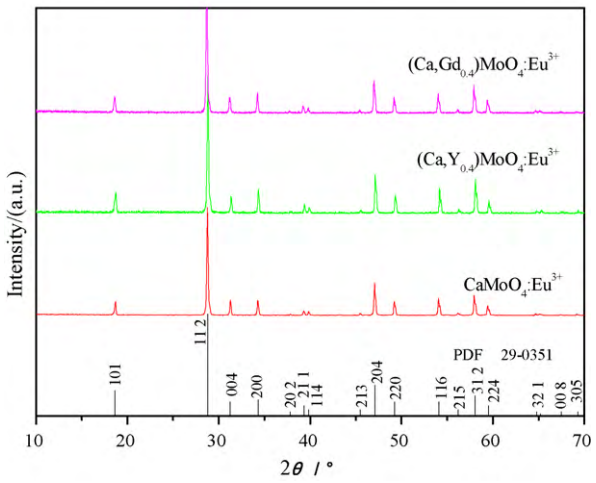

Fig. 1. XRD pattern of the $(Ca,Ln_{0.4})MoO_4$: $0.15Eu^{3+}$ (Ln = Y, Gd) and $CaMoO_4$: $0.15Eu^{3+}$.

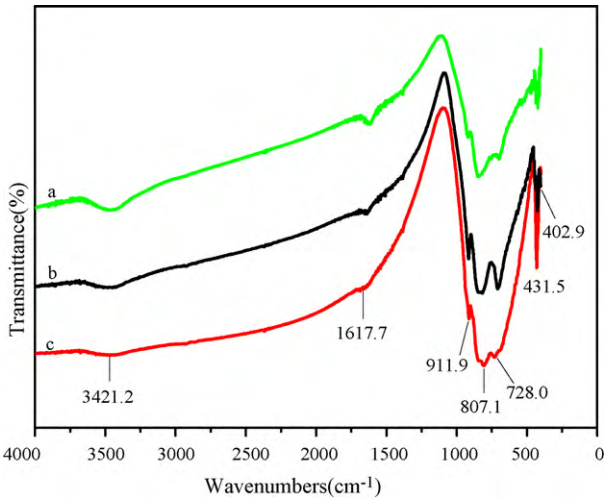

Fig. 2. FT-IR spectra of the $(Ca,Gd_{0.4})MoO_4$: $0.15Eu^{3+}$ (a), $(Ca,Y_{0.4})MoO_4$: $0.15Eu^{3+}$ (b) and $CaMoO_4$: $0.15Eu^{3+}$ (c).

2. Experimental

2.1. Synthesis of $CaLnMoO_4$: Eu^{3+} (Ln = Y, Gd)

Eu_2O_3 (99.99%), $(NH_4)_6Mo_7O_{24}{\cdot}4H_2O$ (A.R.), $Ca(NO_3)_2{\cdot}4H_2O$ (A.R.), $Y(NO_3)_3{\cdot}5H_2O$ (AR)/$Gd(NO_3)_3{\cdot}5H_2O$ (A.R.), NH_4HCO_3 (A.R.), $NH_3{\cdot}H_2O$ (A.R.), HNO_3 (A.R.) were used as the starting materials. The doping concentration of Eu^{3+} takes 15 mol% in $(Ca_{1-x-y},Ln_y)MoO_4$: xEu^{3+} (Ln = Y, Gd). The samples were synthesized as follows: Eu_2O_3 was dissolved in dilute nitric acid with continuous stirring till transparent solution. And the solution was heated in order to evaporate excess nitric acid. Stoichiometric $(NH_4)_6Mo_7O_{24}{\cdot}4H_2O$, $Ca(NO_3)_2{\cdot}4H_2O$, $Y(NO_3)_3{\cdot}5H_2O$/$Gd(NO_3)_3{\cdot}5H_2O$ were respectively dissolved in deionized water, mixed with above solution and formed mother liquor. Using peristaltic pumps (flow 5 mL/min), the mother liquor was dropped in a certain concentration of NH_4HCO_3–$NH_3{\cdot}H_2O$ precipitator by means of anti-drop with continuous stirring and white precipitation obtained. After aging, filtration, washing, drying the white precipitation at 110–120 °C for 12 h, the white precursor was obtained. Then the precursor was presented at 500 °C, calcined at 600–900 °C, uniformly pink powders without milling were obtained.

2.2. Characterization

The XRD of $(Ca_{1-x-y},Ln_y)MoO_4$: xEu^{3+} (Ln = Y, Gd) powders was carried out by Cu $K\alpha$ radiation (λ = 0.15405 nm). The accelerating voltage and emission current were 40 kV and 30 mA, respectively. The data were recorded over the 2θ range of 10–70° with a step width of 8°/min. FT-IR spectra were characterized by MAGNA-IR 550 IR spectrophotometer using the KBr pellet technique. The composition of the samples was analyzed by Mn $K\alpha$ radiation using INCA Eenergy 350 EDS method. PL spectra were measured by RF-5301 Molecular Fluorescence Spectrometer which equipped with xenon lamp as excitation source. The excitation and emission slit was 3 nm. All the measurements were performed at room temperature.

3. Results and discussion

3.1. Crystal structure of $CaLnMoO_4$: Eu^{3+} (Ln = Y, Gd)

Fig. 1 is the XRD pattern of $(Ca,Ln_{0.4})MoO_4$: $0.15Eu^{3+}$ (Ln = Y, Gd) and $CaMoO_4$: $0.15Eu^{3+}$ phosphors which synthesized by co-precipitation method. The pattern shows that all of the samples suit well with the Joint Committee on Powder Diffraction Standards (JCPDS) file 29-0351 of $CaMoO_4$, which owns a single phase with the scheelite structure of space group $I41/a$, indicating that the replacement of Y^{3+} or Gd^{3+} cannot change the lattice site of the host crystal. The approximate particle size of the sample can be calculated by the Scherrer's equation [12],

$$D = \frac{0.89\lambda}{\beta \cos\theta} \quad (1)$$

where D is the average grain size, λ (=0.15405 nm) represents the $Cu\ K\alpha$ wavelength, θ is Bragg angle and β is the full width at half maximum (FWHM). The three XRD peaks of (1 1 2), (2 0 4) and (3 1 2) are used to calculate the mean size of the samples. The calculation shows that the average crystallite size of $CaMoO_4$: Eu^{3+}, $(Ca,Y)MoO_4$: Eu^{3+} and $(Ca,Gd)MoO_4$: Eu^{3+} are 36.8, 37.5 and 39.7 nm, respectively. The difference of the size is due to the fact that the ionic radius of Y^{3+} (0.116 nm) or Gd^{3+} (0.119 nm) is bigger than that of Ca^{2+} (0.114 nm), and the adjacent O^{2-} ions become more discrete and the crystallite size is increased when the site of Ca^{2+} is occupied by Y^{3+} or Gd^{3+}.

The FT-IR spectrum of the $(Ca,Gd_{0.4})MoO_4$: $0.15Eu^{3+}$, $(Ca,Y_{0.4})MoO_4$: $0.15Eu^{3+}$ and $CaMoO_4$: $0.15Eu^{3+}$ phosphors which synthesized by co-precipitation method at 900 °C for 4 h is shown in Fig. 2. It can be seen that the three samples have approximate vibration modes. The weak adsorption bands at 3421.2 and 1617.7 cm^{-1} are owed to O–H stretching vibration and H–O–H bending vibration of physically absorbed water on the sample surface. The strong absorption peaks at 911.9, 807.1 and 728.0 cm^{-1} which are assigned to stretching vibration of O–Mo–O in MoO_4^{2-} tetrahedron. And the adsorption peak at 431.5 and 402.9 cm^{-1} can be corresponded to v_2 bending vibration of Mo–O [13]. It can be also got from the spectra that the peaks of $(Ca,Y)MoO_4$: Eu^{3+} and $CaMoO_4$: Eu^{3+} are shift slightly toward short wavelength compared with $(Ca,Gd)MoO_4$: Eu^{3+}, which indicated that the doped Gd and Y elements has little effect on the structure of phosphor.

3.2. EDS analysis of samples

Fig. 3 gives the EDS of $(Ca,Y_{0.4})MoO_4$: $0.15Eu^{3+}$ and $(Ca,Gd_{0.4})MoO_4$: $0.15Eu^{3+}$ which synthesized at 900 °C for 4 h. The EDS of the $(Ca,Y_{0.4})MoO_4$: $0.15Eu^{3+}$ confirms the presence of calcium (Ca), oxygen (O), molybdenum (Mo), europium (Eu), yttrium (Y), and the approximate surface composition extracted from the EDS analysis gives a weight ratio to Ca, O, Mo, Eu and Y 7.1%, 24.55%, 41.51%, 10.51% and 16.33%, which is much closer to the theoretical value of 7.6%, 27.1%, 40.59%, 9.6% and 15.2%. The EDS analysis also gives the approximate surface composition of the weight ratio to Ca, O, Mo, Eu and Gd in $(Ca,Gd_{0.4})MoO_4$: $0.15Eu^{3+}$ phosphor 5.90%, 25.46%, 36.09%, 7.97% and 24.58%, respectively, coinciding with the theoretical value of 6.84%, 24.27%, 36.37%, 8.64% and 23.86%. The analysis of EDS shows that the red phosphors $(Ca,Y_{0.4})MoO_4$: $0.15Eu^{3+}$ and $(Ca,Gd_{0.4})MoO_4$: $0.15Eu^{3+}$ have been prepared successfully by co-precipitation method.

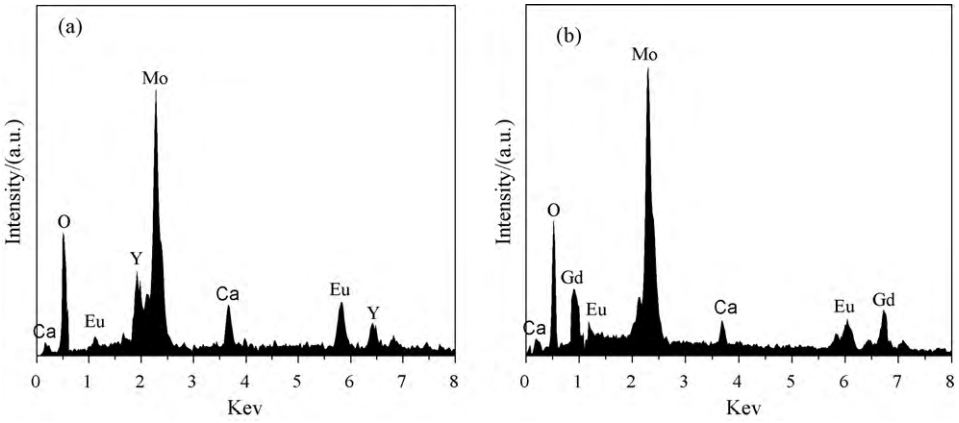

Fig. 3. EDS of $(Ca,Y_{0.4})MoO_4$: $0.15Eu^{3+}$ (a) and $(Ca,Gd_{0.4})MoO_4$: $0.15Eu^{3+}$ (b).

3.3. Photoluminescence properties

The excitation spectra of $CaMoO_4$: $0.15Eu^{3+}$, $(Ca,Y_{0.4})MoO_4$: $0.15Eu^{3+}$ and $(Ca,Gd_{0.4})MoO_4$: $0.15Eu^{3+}$ powders at the monitor of 614 nm is shown in Fig. 4. The three samples show much similar excitation feature except for difference in the intensity. Two broad luminescence band ranges from 240 to 350 nm in the spectrum whose origin of the redistribution of charge density is from 2p orbit of O^{2-} to 4d and 4f molecular orbit of Mo^{6+} and Eu^{3+} [14]. The weak Mo–O charge absorption bands of 240–290 nm is due to the lattice defects which resulted in the replacement of Ca^{2+} by Eu^{3+}, Y^{3+} or Gd^{3+} [15]. However, the defects are favorable in transferring energy from MoO_4^{2-} matrix to Eu^{3+} ion; especially while enhancing the $^7F_0 \rightarrow {}^5D_2$ electronic transition at 465 nm. Compared with the excitation spectra of $CaMoO_4$: Eu^{3+}, the Eu-O charge transfer band of $(Ca,Ln_{0.4})MoO_4$: Eu^{3+}(Ln = Y, Gd) at 300~350 nm observably shifts toward the longer wavelength and have a higher intensity, which is associated with the electron cloud rearrangement effect of Eu^{3+}–O^{2-}. The intensity and location of charge transfer band within M^{2+}–O^{2-}–Eu^{3+} (M = Ca^{2+}) are sensitive to the covalency of M^{2+}–O^{2-} bond. The covalency of Ln^{3+}–O^{2-} bond becomes stronger after Ln^{3+} getting into the lattice sites of Ca^{2+}, which resulted in the decrease of migration energy from the 2p orbital of O^{2-} to the 4f orbital of Eu^{3+}. Thus, the band of charge transfer will be enhanced and lead to red shift. According to the present case, the intensity of charge transfer band is stronger and the wavelength of red shift of Gd^{3+}–O^{2-}–Eu^{3+} is greater than those of Y^{3+}–O^{2-}–Eu^{3+}, which is not the same with the result of literature [16]. Huang et al. [17] finds that the crystal field has an important effect on the center field and then causes the electron cloud expansion effect. Compared with

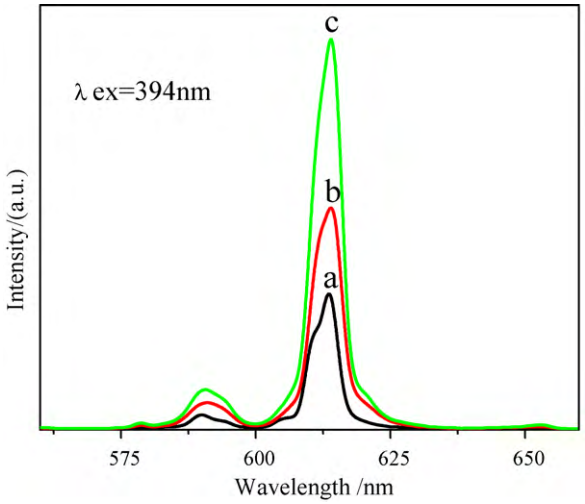

Fig. 5. Emission spectra of $CaMoO_4$: $0.15Eu^{3+}$(a), $(Ca,Y_{0.4})MoO_4$: $0.15Eu^{3+}$(b) and $(Ca,Gd_{0.4})MoO_4$: $0.15Eu^{3+}$(c).

Y^{3+} ion, the bigger radius of Gd^{3+} will probably lead to a larger distortion of the crystal lattice and a lower symmetry. Therefore, the crystal field effect is stronger around the Eu^{3+}, and the intensity of the charge transfer bands and red shift will be bigger than those of $(Ca,Y_{0.4})MoO_4$: $0.15Eu^{3+}$. In addition, the narrow peaks at 362, 383, 394, 425, 465 and 475 nm are the transitions of Eu^{3+} from the ground state to the excited state of $4f^7$ configuration, respectively, corresponding to $^7F_0 \rightarrow {}^5D_4$, $^7F_0 \rightarrow {}^5L_7$, $^7F_0 \rightarrow {}^5L_6$, $^7F_0 \rightarrow {}^5D_3$,

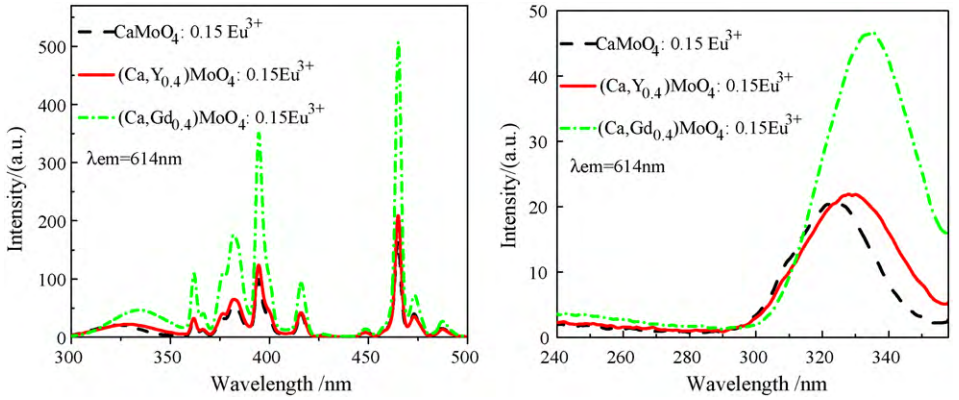

Fig. 4. Excitation spectra of $CaMoO_4$: $0.15\ Eu^{3+}$, $(Ca,Y_{0.4})MoO_4$: $0.15Eu^{3+}$ and $(Ca,Gd_{0.4})MoO_4$: $0.15Eu^{3+}$.

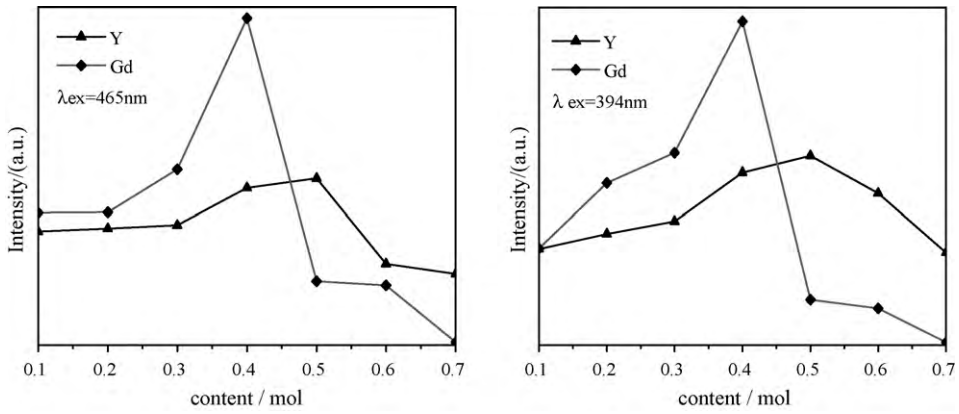

Fig. 6. Effect on the luminescent properties of the different contents of Y and Gd in the red phosphors.

$^7F_0 \rightarrow {}^5D_2$ and $^7F_0 \rightarrow {}^5D_1$ transition. The absorption of $^7F_0 \rightarrow {}^5L_6$ and $^7F_0 \rightarrow {}^5D_2$ are stronger than other peaks, which matches well with the emission wavelength of the UV LED or the blue LED chips, thus improving color rendering property of the commercial W-LED.

Fig. 5 shows the emission spectra of $CaMoO_4$: $0.15Eu^{3+}$, $(Ca,Y_{0.4})MoO_4$: $0.15Eu^{3+}$ and $(Ca,Gd_{0.4})MoO_4$: $0.15Eu^3$ at the excitation of 394 nm. The peak position and shape of the samples are the same except for intensity. The strong red emission around 614 nm is owing to the electric dipole transition $^5D_0 \rightarrow {}^7F_2$, while the weak orange emission located around 590 nm is belonging to the magnetic dipole transition $^5D_0 \rightarrow {}^7F_1$. According to the Judd–Ofelt theory [18], the f–f transitions of $4f^N$ configuration is mainly electric in dipole transition and the magnetic dipole transition. The f–f transition of Eu^{3+} is transition within the f^6 configuration and the start state and final state is the same one, so the electric dipole transition is forbidden. However, in the crystal lattice of $CaMoO_4$: Eu^{3+}, the introduction of Y^{3+} and Gd^{3+} makes the symmetry center of Eu^{3+} move. The opposite configurations of 5d and 5g mixing with 4f configuration lead to the parity forbidden block partially relax and result in the electric dipole transition of $^5D_0 \rightarrow {}^7F_2$. The intensity of $^5D_0 \rightarrow {}^7F_2$ is much stronger than that of the magnetic dipole transition $^5D_0 \rightarrow {}^7F_1$ [12]. Thus the red lights which emit from our sample are much pure. Moreover, because the radius of Gd^{3+} is bigger than that of Y^{3+}, the symmetry of the local environment around Eu^{3+} will be changed greatly after Gd^{3+} doping into the $CaMoO_4$ crystal, and so the parity forbidden block will be relaxed well. And then the intensity of ultra-sensitive electric dipole transition in $(Ca,Gd_{0.4})MoO_4$: $0.15Eu^{3+}$ is significantly higher than that of $CaMoO_4$: $0.15Eu^{3+}$ and $(Ca,Y_{0.4})MoO_4$: $0.15Eu^{3+}$ phosphors.

Fig. 6 shows the effect of the different contents of Y and Gd on luminescent properties excitation at 465 and 394 nm. From Fig. 6, people can find that the intensity of the red light increases with the enhancement of the mole fraction of Y and Gd while it is fewer than 40% and 50%, respectively. But when the mole fraction of Y and Gd over 40% and 50%, respectively, the intensity decreases with the increasing of the dope quantity. In $CaMoO_4$: Eu^{3+} crystal, the lattice seat of Ca^{2+} were replaced by Y^{3+} or Gd^{3+}, and a small amount of doping undermined the integrity of crystal lattice to some extent and caused the imbalance of charge, so the crystal field of the surrounding Eu^{3+} is greater and the parity election law can be relaxed well and the luminous intensity is enhanced. However, the scheelite crystal structure of $CaMoO_4$ will be changed if the doping is too high [19], which leads to the mutation of the luminescent properties and obvious declination of the light intensity.

4. Conclusions

In conclusion, a series of $(Ca_{1-x-y},Ln_y)MoO_4$: xEu^{3+} (Ln = Y, Gd) red phosphors have been prepared by co-precipitation method using NH_4HCO_3–$NH_3{\cdot}H_2O$ as precipitator. The results show that $(Ca_{1-x-y},Ln_y)MoO_4$: xEu^{3+} has a single phase with scheelite structure. The Y, Gd doped in $(Ca_{1-x-y},Ln_y)MoO_4$: xEu^{3+} cannot change the lattice site and the molecular structure of the whole host, but can increase the crystal field around Eu^{3+} ion and enhance the efficiency of electronic absorption at $^7F_0 \rightarrow {}^5L_6$ (394 nm) and $^7F_0 \rightarrow {}^5D_2$ (465 nm) which matches well with the UV and blue LED chips and improves effectively the performance of commercial W-LED. The luminescent intensity of $(Ca_{1-x-y},Ln_y)MoO_4$: xEu^{3+} is obviously higher than that of $CaMoO_4$: Eu^{3+} which is not doping Y or Ga. In addition, the optimal luminescent intensity of the $(Ca_{1-x-y},Ln_y)MoO_4$: xEu^{3+} phosphor powders was obtained when Ca was substituted by 40 mol% Y or 50 mol% Gd.

Acknowledgements

Project supported by the Innovative Talent Training Project of the Third Stage of “211 Project”, Chongqing University (No. S-09103), the Natural Science Foundation of Chongqing (No.2005BA4016) and the National Science Foundation for Postdoctoral Scientists of China (No. 20100470810).

References

[1] T.T. Dong, Z.H. Li, Z.X. Ding, L. Wu, X.X. Wang, X.Z. Fu, Mater. Res. Bull. 43 (2008) 1694.
[2] K.S. Hwang, S. Hwangbo, J.T. Kim, Ceram. Int. 35 (2009) 2517.
[3] Y.G. Wang, J.F. Ma, J.T. Tao, X.Y. Zhu, J. Zhou, Z.Q. Zhao, L.J. Xie, H. Tian, Ceram. Int. 33 (2007) 693.
[4] K. Nassau, P.B. Jamieson, J.W. Shiever, J. Phys. Chem. Solids 30 (1969) 1231.
[5] C.H. Chiu, M.F. Wang, C.S. Lee, T.M. Chen, J. Solid State Chem. 180 (2007) 619.
[6] Y.S. Hu, W.D. Zhuanga, H.Q. Ye, D.H. Wang, J. Alloys Compd. 390 (2005) 226.
[7] F.B. Cao, Y.W. Tian, Y.J. Chen, L.J. Xiao, Q. Wu, J. Alloys Compd. 475 (2009) 387.
[8] Q.M. Wang, B. Yan, Mater. Chem. Phys. 94 (2005) 241.
[9] M.M. Haque, H.I. Lee, D.K. Kim, J. Alloys Compd. 481 (2009) 792.
[10] F. Gao, L.F. Liang, C.F. Cuo, Chin. J. Lumin. 30 (2009) 611.
[11] P. Yang, G.Q. Yao, J.H. Lin, Inorg. Chem. Commun. 7 (2004) 389.
[12] F. Lei, B. Yan, J. Solid State Chem. 181 (2008) 855.
[13] I.L.V. Rosa, A.P.A. Marques, M.T.S. Tanaka, D.M.A. Melo, E.R. Leite, E. Longo, J.A. Varela, J. Fluoresc. 18 (2008) 239.
[14] Z.J. Zhang, H.H. Chen, X.X. Yang, J.T. Zhao, Mater. Sci. Eng. B 145 (2007) 34.
[15] X.G. Wang, S.L. Bo, X.N. Qi, M.L. Li, M. Li, Chin. J. Inorg. Chem. 25 (2009) 350.
[16] Z.L. Wang, H.B. Liang, M.L. Gong, Q. Su, J. Alloys Compd. 432 (2007) 308.
[17] P. Huang, C. Cui, S. Wang, Opt. Mater. 32 (2009) 184.
[18] B. Yan, J.H. Wu, Mater. Chem. Phys. 116 (2009) 67.
[19] J. Liu, H.Z. Lian, C.S. Shi, Opt. Mater. 29 (2007) 1591.